The role of carrier gas flow in roll-to-roll AP-PECVD synthesized silica moisture barrier films

Surface & Coatings Technology 339 (2018) 20–26

Contents lists available at ScienceDirect

Surface & Coatings Technology

journal homepage: www.elsevier.com/locate/surfcoat

The role of carrier gas flow in roll-to-roll AP-PECVD synthesized silica moisture barrier films

A.S. Meshkova[a,b,*], F.M. Elam[a,b], S.A. Starostin[c], M.C.M. van de Sanden[a,b], H.W. de Vries[a]

[a] Dutch Institute for Fundamental Energy Research, P.O. Box 6336, 5600 HH Eindhoven, The Netherlands
[b] Eindhoven University of Technology, P.O. Box 513, 5600 MB Eindhoven, The Netherlands
[c] FUJIFILM Manufacturing Europe B.V., P.O. Box 90156, 5000 LJ Tilburg, The Netherlands

ARTICLE INFO

Keywords:
Atmospheric pressure PECVD
Vertical chemical gradient
Non-uniform deposition rate
Silica barrier film

ABSTRACT

Moisture barrier films are deposited on a polymer foil by roll-to-roll Atmospheric Pressure Plasma Enhanced CVD reactor using a N_2, O_2, TEOS gas mixture. The film microstructure and permeation properties are studied as a function of the carrier gas flow rate with both static and dynamic film transport. The microstructure is analyzed by spatially resolved attenuated total reflectance (ATR)-FTIR and correlated with the vertical density gradient obtained in the dynamic films and the moisture barrier performance. It is shown that by varying the carrier gas flow rate the vertical density gradient, or the network porosity, can be tuned by governing the convective transport inside the reactor consequently densifying the inorganic film at fixed energy cost (i.e. Yasuda parameter) of the process. Moreover, adopting the bilayer architecture allows to achieve the same moisture barrier properties of $2 \cdot 10^{-3}$ g·m^{-2}·day^{-1} (40 °C, 90% RH) at only half the film thickness of a single layer barrier films, which consequently leads to a throughput increase of almost two times.

1. Introduction

The dielectric barrier discharge (DBD) reactor type, widely employed in surface treatment applications [1] is nowadays subject of intense research for the synthesis of functional thin films either in a plane parallel or in a cylindrical electrode geometry [2–9]. In the DBD reactor with the gas mixture injected parallel to the electrodes and operating in precursor deficiency regime, the precursor depletion results in a non-uniform deposition rate profile along the gas flow [10,11]. The chemical composition and density of the layer depends on the local flux of reactive species arriving at the surface. Thus, the properties of the thin films deposited, depend on the exact growth location in the reactor. Therefore, deposition on the moving web produces a vertical gradient (in depth profile in the direction of film growth) in the film properties, which is of interest for numerous thin film applications. For example, in gradient layers combining stress relaxation properties to bridge the difference in density between the organic and inorganic material (providing excellent adhesion to the substrate) with tailored surface properties [11,12]. The tailored surface can be either highly hydrophilic and possess adhesive properties with specific chemical reactive sites, or can be repellent to liquids with hydrophobic or oleophobic properties [13,14]. In addition, the vertical variation in the film properties can be exploited in anti-reflection coatings [15] by creating a gradient in the refractive index, in membrane layers by producing a gradient in the size and inter-connectivity of the porosity or in films with a gradient in the chemical composition for the synthesis of ultra-low moisture barrier films [6,16,17]. In other applications the vertical gradient properties can be highly undesirable, for example, in silicon microstructures used for electronic devices demanding uniform electrical properties [3].

In the present work we concentrate on dense silica-like films deposited on a polymer substrate by a roll-to-roll atmospheric pressure plasma enhanced chemical vapor deposition (AP-PECVD) which despite the intrinsic vertical gradient properties possess a significantly reduced oxygen and water permeation function. These functional foils can therefore be used for the protection of electronic components such as flexible solar cells, optical components like quantum dots or in food and medical packaging applications [18–27]. Effective water vapor transmission rate (WVTR) measurements showed that rates as low as $6.9 \cdot 10^{-4}$ g·m^{-2}·day^{-1} (at 40 °C, 90% RH) can be achieved using a bilayer film architecture [28].

In a recent study [11] the gradient film properties of films deposited on static substrate in an AP-PECVD reactor were investigated using spatially resolved ATR-FITR analysis. As ATR-FTIR has proved to be a valuable technique to study the intrinsic microstructure of amorphous silica films, with a focus on the relative content of hydroxyl (−OH)

* Corresponding author at: Dutch Institute for Fundamental Energy Research, P.O. Box 6336, 5600 HH Eindhoven, The Netherlands.
E-mail address: a.meshkova@differ.nl (A.S. Meshkova).

https://doi.org/10.1016/j.surfcoat.2018.02.010
Received 14 November 2017; Received in revised form 1 February 2018; Accepted 3 February 2018
Available online 04 February 2018

impurities [5,6,29–32]. A clear variation in the film microstructure has been observed within the discharge region. A higher network porosity was observed for a short gas residence time and high precursor partial pressure, while denser layers were deposited in the region with a longer gas residence time and low precursor partial pressure. The network porosity in silica-like films is correlated with the presence of hydroxyl groups in the network structure [6,29–33]. This observation is particularly relevant for the moisture barrier film, because within the discharge region these variable film properties translate into a vertical porosity gradient when the silica films are (dynamically) deposited on a moving substrate. This could provide a means to control the in depth properties of the layers, such as the network porosity [29–33], which has a direct correlation with the moisture barrier properties of the films. Thus, it was demonstrated that the dynamically deposited films are characterized by a vertical gradient in the microstructure, having depth dependent mechanical and moisture barrier properties. The previous study [11] argued that for a single layer moisture barrier with a thickness of about 50 nm, only the top part of the layer of approximately 10–15 nm of silica is significantly contributing to the barrier properties whereas the underlying silica of 35–40 nm provides adhesion to the polymer and assures stress relaxation between the polymer and the dense silica barrier film. From a practical point of view this provides new insight in the possibility to scale the reactor throughput and to increase the production of high quality barrier film. Considering that the energy delivered per precursor molecule [5] should remain constant (in analogy to the similarity defined by the Yasuda parameter [34]), an increase in the throughput means an increase in reactive gas flow rates with proportional increase in power dissipated in the plasma. However, in practice this straightforward approach has limitations such as the dependency of the DBD regime on the dissipated power density, thermal sensitivity of the polymeric substrates and a limited length of the reactive plasma zone. At the same time both the dynamic deposition rate and specific energy spent per precursor molecule, as discussed in [5], represents averaged values in the PECVD reactor. Hence, the local deposition rate as well as the local plasma chemical kinetics significantly varies along the gas flow direction due to the precursor depletion. It was earlier suggested by Starostin et al. [35] that the scaling of the AP-PECVD reactor throughput for a moisture barrier layer strongly depends on the non-uniform deposition rate profile along the gas flow. As the active plasma region is rather limited and only a small portion of the total film thickness is contributing to the barrier film functionality, a more uniform deposition rate profile may thus increase the portion of the silica film that contributes to the barrier properties.

The question addressed is, how the vertical gradient in the film properties can be exploited to reduce the network porosity and improve the SiO_2 barrier film properties. In this context, the present work is a step forward in tailoring the network porosity in the films by varying the carrier gas flow meaning controlling the convective transport of precursor fragments while keeping fixed energy cost of the process. A comprehensive analysis is carried out of how the gradient in the silanol concentration, induced by changing the carrier gas flow rate, is related to the moisture barrier films. In addition the role of the gas flow rate on the moisture barrier performance in a single and a bilayer architecture [22–26,36–38] is systematically investigated.

2. Experimental section

The experimental roll-to-roll reactor for thin film deposition was already described in detail elsewhere [5]. In brief, the system consisted of cylindrical electrodes in a bi-axial geometry, a gas injector and an independent foil transport system. The dielectric barrier discharge was ignited between the two metal rotary drum electrodes with radii of 120 mm. Both electrodes were covered by dielectric foils. On the bottom electrode polyethylene-2,6-naphthalate (PEN) foil was used and a sacrificial foil (ASTERA™ Functional Foils, AGFA Polyethylene terephthalate) was used for the top electrode. The PET was transported at a constant line speed of 50 mm·min^{-1}. The discharge was sustained by applying an AC high voltage of approximately 2–3 kV in a frequency range between 180 and 215 kHz. The experimental conditions were selected based on our previous work [5], i.e. dynamically deposited 100 nm thick silica films having a WVTR of $2 \cdot 10^{-3}$ g·m^{-2}·day^{-1} at 40 °C, 90% RH. The dissipated power in the discharge was 575 W, as calculated from the current voltage characteristic [5], corresponding to an approximate power density of 19.2 W·cm^{-2} (taking a characteristic discharge expansion length of 20 mm for the described experimental conditions). The discharge width was 15 cm and the smallest gaseous gap was 0.5 mm. Oxygen was used as an oxidizer and argon as an inert mixing gas to carry the precursor vapor in the controlled evaporation mixer unit. Nitrogen was used as the carrier gas and the flow rate (Q) was varied between 5 and 40 slm meanwhile oxygen and tetraethyl orthosilicate (TEOS) precursor for the silica layers were kept constant at flow rates of 0.5 slm and $1.8 \cdot 10^{-3}$ slm, respectively. The nitrogen flow rate of 18 slm was used as a reference condition for direct comparison with the previous study [5,11].

Two types of deposition modes were utilized in this work. The 'static mode' without foil transport and deposition took place just in the discharge region, and the 'dynamic mode' when the foil was transported in the same direction as the gas flow and a uniform film thickness was deposited. The static films were deposited for 60 s on a silica buffer layer which served as a protective layer to prevent any plasma interaction with the bare PEN foil [4]. The silica buffer was deposited at a precursor flow of $8.2 \cdot 10^{-3}$ slm and a web speed of 800 and 400 mm·min^{-1}, to prepare a thin protective layer of 20 and 40 nm [11,39]. For the WVTR measurements two types of dynamic films were deposited single barrier films and bilayer barrier films. The web speed for the single films was 60 mm·min^{-1} and for the bilayer films 110 mm·min^{-1}, aiming for a film thickness of 80 and 40 nm, respectively. Hence, the bilayer architecture of the film comprised of a 40 nm buffer layer and a 40 nm silica barrier film to exclude thickness effects when the WVTR is compared. A schematic architecture of the single barrier films and bilayer films is shown in Fig. 1.

The film thickness of SiO_2 profiles was measured using a focused beam spectroscopic ellipsometry (SE) (M-2000D, J.A. Woollam Inc.) in the wavelength range of 245–1000 nm with 120 μm spot size of the beam. The SE was equipped with a translation table which allowed space resolved measurement of the static samples in the range of −20 mm to 20 mm over 641 points with a step of 0.1 mm. To describe the PEN substrate and the silica-like film a Cauchy dispersion function was applied for both materials. The substrate anisotropy was not

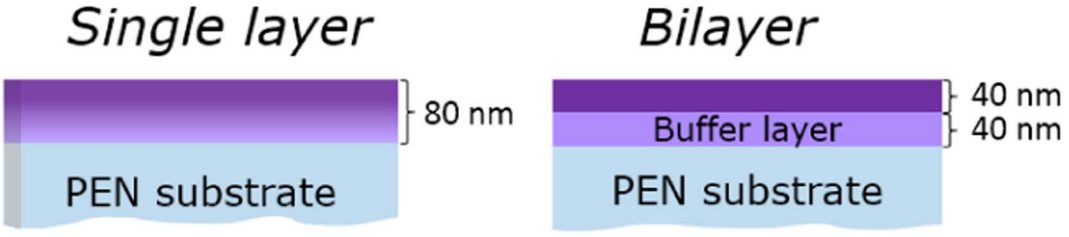

Fig. 1. A schematic representation of the silica-like layer in the single and bilayer architecture. (For interpretation of the references to color in this figure, the reader is referred to the web version of this article.)

implemented into the model [40], however the sample orientation was kept the same for each measurement.

To clarify the role of the local deposition rate on the film morphology spatially resolved Attenuated Total Reflectance (ATR)-FTIR was performed on the statically deposited silica-like films. The IR absorption spectra were acquired over 8 scans from 650 to 4000 cm^{-1} using the Perkin Elmer Frontier (Frontier FT-IR/FIR Spectrometer, PerkinElmer; Frontier UATR Ge/Ge, PerkinElmer). This set-up utilized a Ge crystal with a 45° face angle and one internal reflection. The spatial resolution of the crystal is 1 mm. Deconvolution of all spectral peaks was carried out (Peak Analyzer – Fit Peaks (Pro), OriginPro 9.1) in order to determine absorbance intensity of each individual contribution. The detailed ATR-FTIR analysis was described elsewhere [11].

A Mocon Aquatran Model 1 was used to measure the overall Water Vapor Permeation Rate (WVTR) with set conditions of 40 °C, 90% RH. The minimum detection limit of this system is $5 \cdot 10^{-4}$ $g \cdot m^{-2} \cdot day^{-1}$ and the sample area is 50 cm^2. The WVTR was recorded after the value reached equilibrium with an average measurement time of 71 h.

The macro defects such as pinholes were resolved in the dynamic series for the single layer and bilayer films by means of the solvent vapor exposure test. In this test the silica films were exposed to a solvent vapor and in the case of pinhole defects locally enhanced diffusion of the vapor induces a local swelling of the PEN leading to the formation of blisters [41]. The exposure time was kept at 5 h for all the samples. Interferometric microscopy (IM) (Wyko NT9100 Optical Profiling System, Veeco Instruments Inc.) was then carried out on the films post-exposure to detect for the presence of blisters and hence for macro-defects in the silica-like films. The IM measurement was performed in phase-shift interferometry mode, analyzing an area of 47 × 63 μm^2. Micrographs were then processed and stitched to form images with areas of 25 mm^2 using the Wyko Vision software. In total, an area of 250 mm^2 was evaluated, for each sample and based on this area the defect density was determined.

3. Results and discussion

3.1. Static profile analysis

A systematic analysis of the static films over a wide range of nitrogen carrier gas flow rates (5 to 40 slm) is carried out. With a gas flow rate of (Q) 5 slm the discharge is visually unstable which is also reflected in variation of the voltage current measurements. At higher gas flows, between 10 and 40 slm, the discharge appears stable and uniform. The thickness profiles are measured using the focused beam SE and the results are presented in Fig. 2 as the local deposition rate (LDR). The zero position on the x scale of the profiles indicates the smallest gap distance between the cylindrical electrodes. By integrating the LDR profile over the deposition length in the electrode space the actual growth front of a dynamically deposited film can be deduced as the dashed lines in Fig. 2. It is clear from Fig. 2 that the shape of the LDR profiles is strongly affected by the gas flow rate. At Q = 5 slm a spatially condensed deposition is obtained which is characterized by a very narrow thickness profile (7 mm) relatively far away from the zero position. Moreover, the dynamic deposition rate is relatively low compared to the higher gas flow rates which can be a sign of the discharge instability for this condition. At Q = 10 slm the total width of the thickness profile increases to approximately 12 mm whereas, the profiles with higher nitrogen flow result in a progressive flattening and increase of the width of the thickness profile. Hence, the local deposition rate decreases less steep after the maximum. The strong influence on the shape of the deposition profile can be explained by the fact that the convective transport of precursor and its fragments along the gas flow direction will be higher as the nitrogen flow increases, while the diffusive transport towards the walls remains the same. Enhancement of the convection over the diffusion results in a flattening of the deposition profile or, a higher gas flow results in an overall decrease of the local

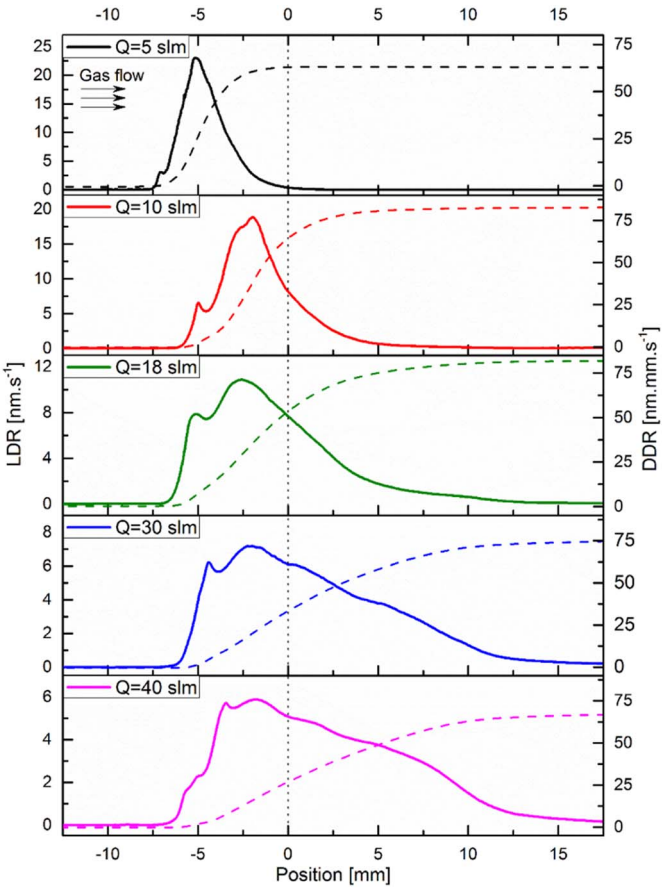

Fig. 2. Local deposition rate profiles of static depositions with a variation in the nitrogen flow rate of 5 to 40 slm. On the right axis the dashed line indicates the accumulative dynamic deposition rate (DDR) value which is comparable to the growth front in the dynamic mode of the DBD reactor.

deposition rate. As earlier reported by [11] two maximums can be observed in the deposition rate profile for all nitrogen gas flows. Remarkably, the local deposition rate of the first maximum is more or less constant, between 5 and 7 $nm \cdot s^{-1}$, whereas the second maximum (main peak) is strongly dependent on the carrier gas flow, see Fig. 2. The precursor flow is kept constant and as a consequence the dynamic deposition rate (DDR) value which is defined as the product of film thickness and web transport speed is constant and independent of carrier gas flow. Because the power density remains unvaried, the specific energy delivered per precursor molecule (related to Yasuda parameter) is constant. For the current experimental conditions the DDR is around 75 to 80 $nm \cdot mm \cdot s^{-1}$ (for Q = 10–30 slm) and the estimated energy spent per TEOS molecule is 6.5 keV/molecule, the specifics of the calculation can be found in [5,28]. The gradual decrease in the calculated DDR value from the static profiles with increasing gas flow is mainly attributed to a slight increase in the gas loss due to stronger convection, see Fig. 2.

As the presence of the hydroxyl groups disrupts the continuous −Si−O−Si−O− network structure [29–32,42] the concentration of hydroxyls has a significant impact on the moisture barrier quality. To estimate the variation in the local film microstructure for different carrier gas flows spatially resolved ATR-FTIR spectroscopic analysis was performed on the profiles shown in Fig. 2. Three representative flow rates of the carrier gas were selected for spatially resolved ATR-FTIR analysis. In Fig. 3 the ATR-FTIR spectra of the static profiles are shown at different positions along the gas flow direction for Q = 10, 18 and 30 slm in the region of hydroxyl stretch between 3000 and 4000 cm^{-1}.

The gradual decrease in the hydroxyl stretch absorption as a

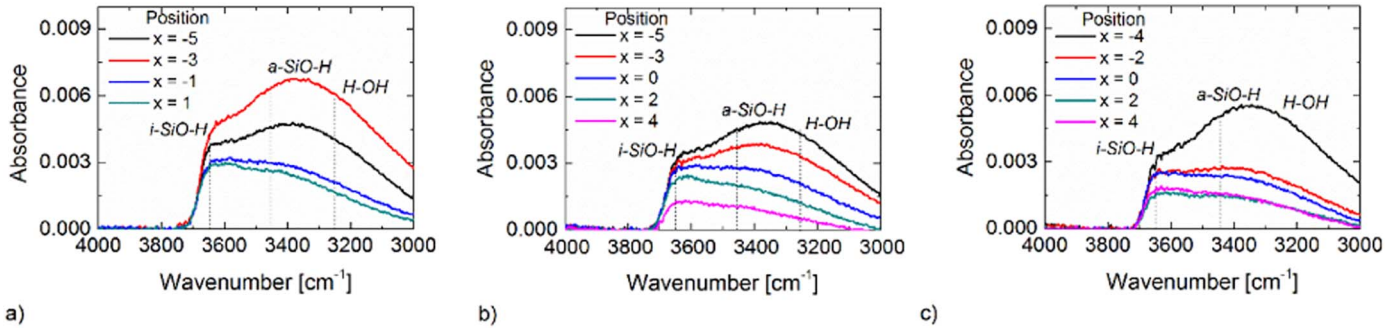

Fig. 3. ATR-FTIR spectra of silica-like film probed at different positions, x, in the static deposition profile in the wavenumber range of 3000–4000 cm^{-1} for a) Q = 10 slm; b) Q = 18 slm and c) Q = 30 slm. The broad peak in this wavenumber range consists of a superposition of three peaks: 1) at 3250 cm^{-1} associated −OH from absorbed water in the film 2) at 3450 cm^{-1} attributed to associated silanol (a-SiO-H) groups and 3) at 3650 cm^{-1} attributed to isolated silanol (i−SiO−H) groups [32,43–45]. The positions (x) of the spectra represented in different colors refer to the positions in the static profiles of Fig. 1. The gas flow direction is always fixed from left to right.

function of the position indicates a decrease in silanol density, which in turn is an indication of a decrease in the network porosity. As can be seen in Fig. 3 the gradient in the silanol concentration is present for all the investigated conditions. Moreover, the change in the LDR profile with the gas flow rate goes along with a redistribution of the silanol concentration in the thickness profile. The absorbance spectra of SiO_2 film deposited at 10 slm of nitrogen shows the highest silanol concentration ([OH]) at the position of the maximum value of the LDR. Notable is that the silanol concentration at the position of the first maximum (with LDR = 5–7 nm·s^{-1}) is more or less independent of the carrier gas flow rate.

The hydroxyl stretch region, in the 4000–3000 cm^{-1} range, is known to include three peaks. An isolated silanol peak at 3650 cm^{-1}, an associated silanol peak at 3450 cm^{-1} and the H−OH stretch peak attributed to interaction with adsorbed water on the sample at 3250 cm^{-1} [32,43–45]. The spectra depicted in Fig. 3 were deconvoluted according to these peak positions, see Fig. 4. In Fig. 4 the absorbance of each individual hydroxyl stretch is portrayed as a function of the relative thickness (of about 80 nm) in the barrier layer if projected as a deposition in the dynamic mode with a line speed of 60 mm·min^{-1}. From Fig. 4 a clear gradient in the hydroxyl group distribution in the vertical direction (from the bottom to the top of the film) can be observed for the different gas flow rates. An exception is the static profile deposited at Q = 10 slm see Fig. 4(a) where the hydroxyl concentration ([OH]) is the highest at the maximum LDR. Here, the deviation in the drop of the [OH] at the positions of −5 and −3 mm can be related to a significant difference in the LDR. It should be realized that the density difference between the top and the bottom of the silica film is always the same for a given deposition condition, and the gradient in the [OH] in the film will be controlled by the line speed or the film thickness (z), according to d[OH]/dz.

As the practical objective of the work is to improve the moisture barrier properties, the aim is to synthesize films with the lowest possible silanol content, which can be achieved by tuning the carrier gas flow rate. The approach is to correlate the local silanol concentration for different gas flow rates with dynamically deposited films assuming a film thickness of 80 nm. The gradient silanol concentration of the films in the dynamic mode is reconstructed based on the static profiles, see Fig. 4. Although the transition in the film properties will not be discrete the film synthesized with a flow rate of 10 slm results in a thick porous layer of around 55 nm and a thinner and denser top layer of ~25 nm. The local silanol profile for a gas flow rate of 18 slm is characterized by the most gradual transition from a porous layer to around 20–25 nm of a dense top-layer. Further increase of the gas flow rate to 30 slm leads to a thinner porous bottom layer and a thicker about 50 nm dense top layer. Hence, it can be assumed that based on the spatially resolved ATR-FTIR analysis of the microstructure the films deposited at a gas flow rate of 30 slm and higher will have the best moisture barrier properties due to the reduced porosity in the integrated film profile. It is worthwhile to mention that the specific energy delivered per precursor molecule is kept constant and only the convective transport of fragments within the discharge is increased due to higher carrier gas flow.

3.2. Dynamically deposited films

The silica like layers with a thickness of 75 ± 3 nm are deposited in a single step and the effective WVTR is measured as a function of the carrier gas flow rate as shown in Fig. 6. The best performing moisture barrier layer is obtained for Q = 18 slm while at a gas flow rate of 10 and 30 slm the moisture barrier performance is worse. However, based on the trend in the intrinsic porosity the best performing moisture barrier layers should be obtained at Q = 30 slm and higher, see Fig. 4(a, c). As the Mocon apparatus characterizes the effective WVTR, the type of permeation channels determining the moisture barrier performance is not taken into account, i.e. intrinsic porosity, nano defects or large pinholes defects [5,18,22–24,27,40,41,46], and thus the origin of the decrease in the effective barrier performance may be different. In order to determine whether pinholes are responsible for the degraded moisture barrier performance the solvent vapor penetration test analysis is performed on the 80 nm single barrier films. The result of the pinhole defect analysis is shown in Fig. 5.

The IM micrographs depict a very clear presence of blisters for different gas flow rates. The highest density of defects is observed at Q = 5 slm which can be attributed to the discharge instability and consequently high degree of filamentation. A low defect density is observed in the case of Q = 10 slm when a relatively thick porous interface layer is formed and the moisture permeation is dominantly controlled by the network porosity. At Q = 18 and 25 slm the WVTR gradually improves due to the decrease in the [OH] and thus decrease in the network porosity while the defect density remains low. Remarkably at Q = 30 and 40 slm the defect density increases 2 orders of magnitude which is also reflected in a gradual increase in the effective WVTR. The number of blisters are quantified and plotted in Fig. 6.

To further investigate the role of the defect formation mechanism at higher gas flows the bilayer architecture is investigated [5,39]. A porous so-called buffer layer is first deposited on the PEN substrate followed by a barrier layer deposited at different carrier gas flow rate Q = 5 to 40 slm. The total thickness of the bilayer is 82 ± 4 nm consisting of approximately 40 nm of buffer layer and 40 nm of dense barrier layer. It should be mentioned here that in this study the thickness of the buffer and barrier layer are not optimized.

The effective WVTR of the bilayer film architecture is shown in Fig. 7. By increasing the carrier gas flow up to 30 slm a WVTR = $2 \cdot 10^{-3}$ g·m^{-2}·day^{-1} can be achieved for an effective barrier thickness of only 40 nm as the buffer layer is essentially characterized by a non-existent moisture barrier with a WVTR = 1 g·m^{-2}·day^{-1} [39].

Moreover, the density of pinhole defects in the bilayer is

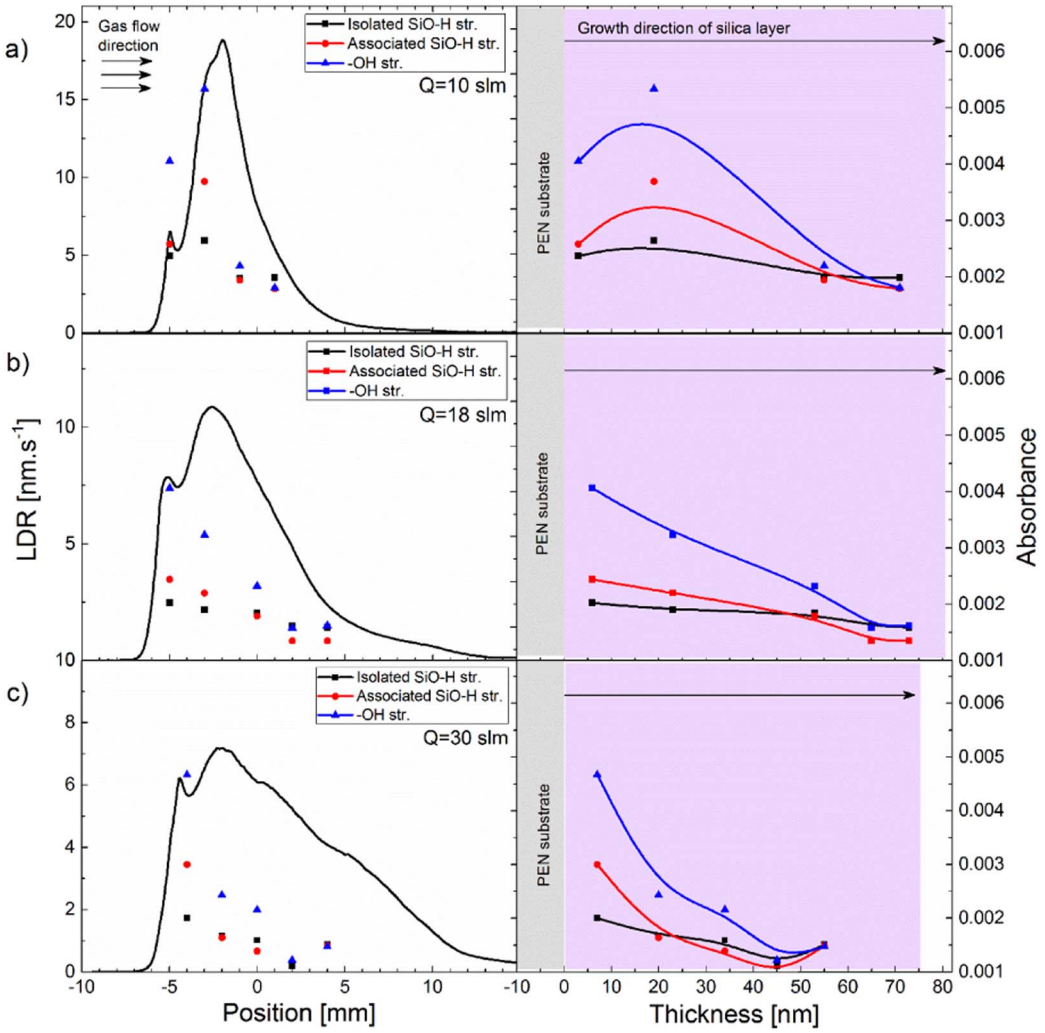

Fig. 4. Deconvolution of the ATR-FTIR absorption spectra shown in Fig. 2: a) Q = 10 slm; b) Q = 18 slm and c) Q = 30 slm of nitrogen. The graph on the left side shows the absorbance as a function of the position (x) in the static profile in the reactor; on the right side the absorbance is shown as a function of the relative film thickness of the samples if projected as a deposition in the dynamic mode with a line speed of 60 mm·min^{-1}.

independent of the gas flow rate, see Fig. 7. The porous interface layer is therefore extremely important for the final quality of the moisture barrier and cannot be neglected. In general, it can be concluded that the moisture permeation at low gas flows is governed by a poor Si—O—Si network structure, see Fig. 4. At higher gas flow rates the Si—O—Si network becomes more crosslinked (having much lower [OH]). The effective WVTR is most probably limited to $2 \cdot 10^{-3}$ g·m^{-2}·day^{-1}, due to the presence of a low density of pinhole defects whereas the residual porosity is further decreased. These pinhole defects can origin from the polymer surface and the buffer layer deposition process. From the polymer surface it can be induced by surface flaws (scratches, particles, pinholes, etc.). Notable is that the defect density appears to be constant and the varying gas flow rates used for the barrier layer do not affect the density of pinhole defects, see Fig. 7. Based on the pinhole calculation model of A.S. da Silva Sobrinho et al. [47] the pinhole size is estimated to be > 20 μm in the bilayer architecture assuming pinhole controlled moisture permeation.

In the single barrier layer case at higher gas flow rates a particularly strong increase in the defect density is observed at Q = 30 and 40 slm. The increase in density of small (~1 μm) pinhole defects [28] must be the main reason for the gradual deterioration of the WVTR values for Q > 25 slm.

In the previous work of [11] it was concluded that the intrinsic buffer layer (acting as a stress relaxation layer) plays a significant factor

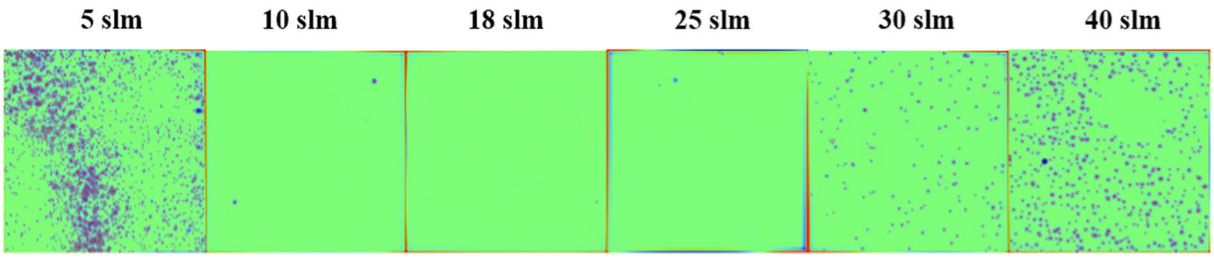

Fig. 5. IM micrographs of blisters developed due to solvent vapor exposure of dynamically deposited layers for single layers with varying gas flow rates of 5–40 slm. The image size is 5 × 5 mm^2.

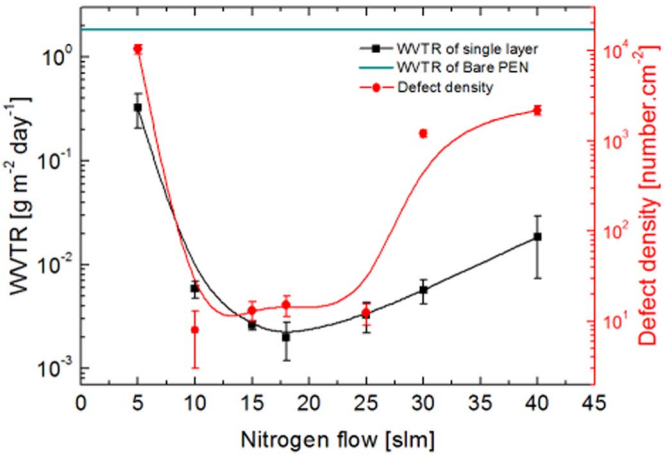

Fig. 6. Effective WVTR (black line) and corresponding defect density (red line) with respect to the nitrogen gas flow rate of single layers. The WVTR of bare PEN foil is indicated as a solid green line. (For interpretation of the references to color in this figure legend, the reader is referred to the web version of this article.)

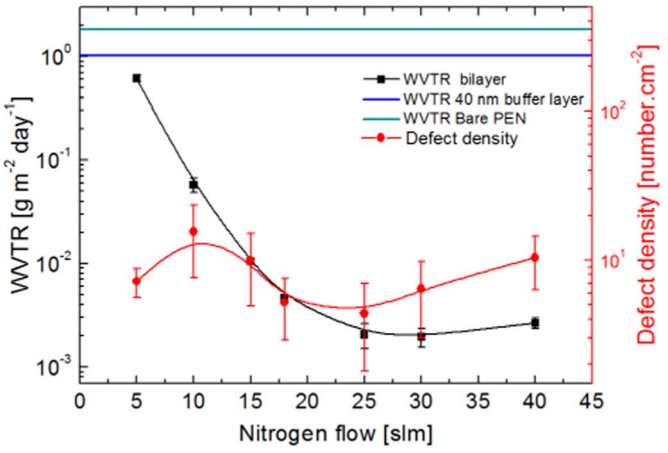

Fig. 7. Effective WVTR (black line) and corresponding defect density (red line) with respect to the nitrogen gas flow rate for the bilayer film architecture. The WVTR of bare PEN foil is indicated as a solid green line. The WVTR of the buffer layer is indicated as a blue line. (For interpretation of the references to color in this figure legend, the reader is referred to the web version of this article.)

in the integrity of the layer by forming a transition layer between the low density PEN substrate and the dense SiO_2 film. Alternatively, it cannot be excluded that during the initial phase of the film growth there is a competition between deposition and etching of the substrate by non-depositing radicals produced in the plasma. If the foil transport direction opposes the gas flow direction a reverse density gradient within the layer will be formed. As a result the first dense part of the layer facing the polymer support will have a very poor adhesion [11]. Interestingly enough by depositing a buffer layer prior to the deposition of a dense barrier layer solves the problem and the barrier film adhesion is independent of the foil transport direction and gas flow direction.

Considering the arguments above for the single layer the mechanism of permeation is highly dependent on the gas flow variation. A first regime is characterized by a porosity controlled permeation at Q = 10 slm (with a pore size of < 1 nm). In a second regime from Q = 15–25 slm the barrier is defect controlled by a low density of presumably substrate defects with a pore size of > 20 μm and a third regime at Q = 30 slm and higher, the layer is controlled by process induced pinholes (size 0.5–1 μm). The possibility to increase the throughput of the process becomes evident and can be enhanced by adjusting the carrier gas flow to synthesize a silica layer with the desired vertical silanol profile gradient. For comparison the moisture

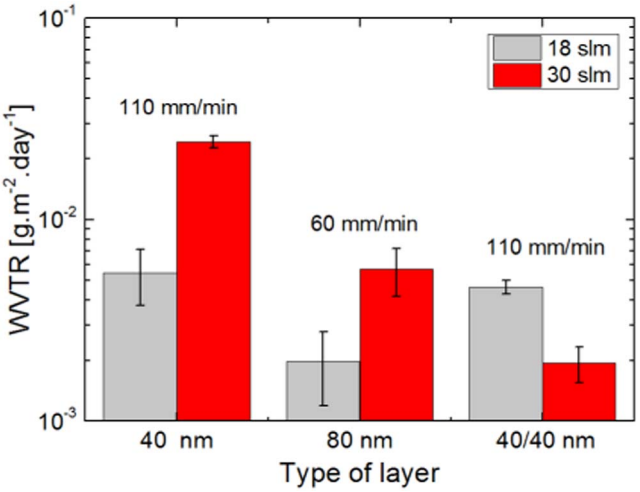

Fig. 8. Comparison of the WVTR for the gas flow rate of 30 slm to the reference gas flow rate of 18 slm for 3 types of layers (sets of bars). The first set of bars the single 40 nm thick films deposited at a web speed of 110 mm·min^{-1}; the second set of bars the single 80 nm thick films deposited at 60 mm·min^{-1} and the third set of bars with the bilayers consisting of 40 nm buffer layer with 40 nm barrier layer, deposited at 110 mm·min^{-1}.

barrier properties of a 40 nm single layers for Q = 18 and 30 slm are assessed in Fig. 8. The 40 nm single layers deposited at 110 mm·m^{-1} have a worse barrier performance. This is confirmed by the abundance of pinhole defects for barriers deposited with increased flow rates, see Fig. 6. Hence, an increase in the throughput by almost a factor of 2 becomes evident for the bilayer in Fig. 8. Therefore, the scaling of the AP-PECVD reactor throughput for the processing of moisture barrier films strongly depends on the non-uniform deposition rate profile along the gas flow. The specific energy per precursor molecule should always be related to the convective transport of the depositing species in order to connect the specific energy per precursor molecule to the functional (i.e. moisture barrier) film properties [48,49].

4. Conclusions

From the spatially resolved ATR-FTIR a non-uniform deposition rate profile with a gradient in the chemical composition is observed for different carrier gas flows with a decrease in the silanol content for increasing carrier gas flow rates. This finding makes control of a vertical density gradient in the film properties via carrier gas flow rate variation possible while keeping the energy cost of the process constant. Although the overall silanol concentration continuously decreases with the gas flow the best performing single layer barrier film is observed for a carrier gas flow of 18 slm. However, the increased gas flow rates carries the penalty of a decreased local deposition rate which leads to undesired effects like etching and the formation of defects. Therefore, three types of permeation causes were identified. The effective WVTR is controlled by the intrinsic porosity for low carrier gas flows, by a low density of large pinhole defects presumably from the substrate for gas flows up to 25 slm and for gas flows of 30 slm and higher the permeation is mainly controlled by process induced pinholes. Thus, a porous interface layer is essential for the deposition of a good barrier film. By adopting a bilayer architecture in order to exclude detrimental plasma polymer interactions it is shown that the carrier gas flow rate can control the gradient film structure and overall barrier permeation properties by controlling intrinsic porosity and formation of the pinholes.

The scaling of the moisture barrier film throughput can be achieved by adjusting the non-uniform deposition rate profile by controlling the gas flow rate. These conclusions can have large impact on the industrial roll-to-roll production of functional SiO_2 thin films. Not only can AP-PECVD be used as an effective production method without the need for

large low pressure set-ups, but by tuning the gas flow rate the throughput can be almost doubled while the same moisture barrier properties can be obtained. As a result a reference WVTR of $2 \cdot 10^{-3}$ g·m^{-2}·day^{-1} is achieved for half the thickness of a non-optimized film by increasing the gas flow rate.

The findings of this study will be relevant for DBD reactors of similar type with the gas and precursor injection parallel to the electrodes, particularly in the case of full depletion of the precursor in the reactor.

Acknowledgements

The presented study was performed in the frame of the Industrial Partnership Programme i31 (APPFF) that is carried out under an agreement between FUJIFILM Manufacturing Europe B.V. and FOM, which is part of the Netherlands Organisation for Scientific Research (NWO). The authors would like to thank Bart van Loon for help with the analysis. The authors are also grateful to Rinie van Beijnen and Emile Gommers (FUJIFILM Manufacturing Europe B.V., Tilburg, The Netherlands) for their technical assistance.

References

[1] U. Kogelschatz, Dielectric-barrier discharges: their history, discharge physics, and industrial applications, Plasma Chem. Plasma Process. 23 (2003) 1–46.
[2] F. Massines, N. Gherardi, A. Fornelli, S. Martin, Atmospheric pressure plasma deposition of thin films by Townsend dielectric barrier discharge, Surf. Coat. Technol. 200 (2005) 1855–1861.
[3] H. Kakiuchi, H. Ohmi, T. Yamada, S. Tamaki, T. Sakaguchi, W. Lin, K. Yasutake, Characterization of Si and SiO, Phys. Status Solidi A 212 (2015) 1571–1577.
[4] P.A. Premkumar, S.A. Starostin, H. De Vries, R.M.J. Paffen, M. Creatore, T.J. Eijkemans, P.M. Koenraad, M.C.M. van de Sanden, High quality SiO_2-like layers by large area atmospheric pressure plasma enhanced CVD: deposition process studies by surface analysis, Plasma Process. Polym. 6 (2009) 693–702.
[5] S.A. Starostin, M. Creatore, J.B. Bouwstra, M.C.M. van de Sanden, H.W. De Vries, Towards roll-to-roll deposition of high quality moisture barrier films on polymers by atmospheric pressure plasma assisted process, Plasma Process. Polym. (2015) 545–554.
[6] J. Petersen, J. Bardon, A. Dinia, D. Ruch, N. Gherardi, Organosilicon coatings deposited in atmospheric pressure Townsend discharge for gas barrier purpose: effect of substrate temperature on structure and properties, ACS Appl. Mater. Interfaces (2012) 5872–5882.
[7] F. Fanelli, Thin film deposition and surface modification with atmospheric pressure dielectric barrier discharges, Surf. Coat. Technol. 205 (2010) 1536–1543.
[8] A. Sonnenfeld, T.M. Tun, L. Zajíčková, K.V. Kozlov, H.-E. Wagner, J.F. Behnke, R. Hippler, Deposition process based on organosilicon precursors in dielectric barrier discharges at atmospheric pressure—a comparison, Plasmas Polym. 6 (2001) 237–266.
[9] H.-E. Wagner, R. Brandenburg, K.V. Kozlov, A. Sonnenfeld, P. Michel, J.F. Behnke, The barrier discharge: basic properties and applications to surface treatment, Vacuum 71 (2003) 417–436.
[10] I. Enache, H. Caquineau, N. Gherardi, T. Paulmier, L. Maechler, F. Massines, Transport phenomena in an atmospheric-pressure Townsend discharge fed by N_2/N_2O/HMDSO mixtures, Plasma Process. Polym. 4 (2007) 806–814.
[11] A.S. Meshkova, Y. Liu, F.M. Elam, S.A. Starostin, M.C.M. van de Sanden, H.W. de Vries, The role of the gradient film properties in silica moisture barriers synthesized in a roll-to-roll atmospheric pressure plasma enhanced CVD reactor, Plasma Process. Polym. 15 (2018), http://dx.doi.org/10.1002/ppap.201700093.
[12] Y. Leterrier, Durability of nanosized oxygen barrier coatings on polymers, Prog. Mater. Sci. 48 (2003) 1–55.
[13] D. Hegemann, C. Oehr, A. Fischer, Design of functional coatings, J. Vac. Sci. Technol. A 23 (2005).
[14] D. Hegemann, H. Brunner, C. Oehr, Plasma treatment of polymers for surface and adhesion improvement, Nucl. Instrum. Methods Phys. Res., Sect. B 208 (2003) 281–286.
[15] L. Martinu, D. Poitras, Plasma deposition of optical films and coatings: a review, J. Vac. Sci. Technol. A 18 (2000) 2619–2645.
[16] M. Yan, T.W. Kim, A.G.G. Erlat, M. Pellow, D.F. Foust, J. Liu, M. Schaepkens, C.M. Heller, P.A. Mcconnelee, T.P. Feist, A.R. Duggal, A transparent, high barrier, and high heat substrate for organic electronics, Proc. IEEE 93 (2005) 1468–1477.
[17] M. Schaepkens, T.W. Kim, A. Gün Erlat, M. Yan, K.W. Flanagan, C.M. Heller, P.a. McConnelee, Ultrahigh barrier coating deposition on polycarbonate substrates, J. Vac. Sci. Technol. A 22 (2004) 1716.
[18] D. Pappas, Status and potential of atmospheric plasma processing of materials, J. Vac. Sci. Technol. A 29 (2011) 20801.
[19] D. Merche, N. Vandencasteele, F. Reniers, Atmospheric plasmas for thin film deposition: a critical review, Thin Solid Films 520 (2012) 4219–4236.
[20] L. Bárdos, H. Baránková, Cold atmospheric plasma: sources, processes, and applications, Thin Solid Films 518 (2010) 6705–6713.
[21] A.B. Chwang, M.A. Rothman, S.Y. Mao, R.H. Hewitt, M.S. Weaver, J.A. Silvernail, K. Rajan, M. Hack, J.J. Brown, X. Chu, L. Moro, T. Krajewski, N. Rutherford, Thin film encapsulated flexible organic electroluminescent displays, Appl. Phys. Lett. 83 (2003) 413–415.
[22] Y.C. Han, E. Kim, W. Kim, H.G. Im, B.S. Bae, K.C. Choi, A flexible moisture barrier comprised of a SiO_2-embedded organic-inorganic hybrid nanocomposite and Al_2O_3 for thin-film encapsulation of OLEDs, Org. Electron. Phys. Mater. Appl. 14 (2013) 1435–1440.
[23] A. Morlier, S. Cros, J.P. Garandet, N. Alberola, Gas barrier properties of solution processed composite multilayer structures for organic solar cells encapsulation, Sol. Energy Mater. Sol. Cells 115 (2013) 93–99.
[24] J. Lewis, Material challenge for flexible organic devices, Mater. Today 9 (2006) 38–45.
[25] M.S. Weaver, L.A. Michalski, K. Rajan, M.A. Rothman, J.A. Silvernail, J.J. Brown, P.E. Burrows, G.L. Graff, M.E. Gross, P.M. Martin, M. Hall, E. Mast, C. Bonham, W. Bennett, M. Zumhoff, Organic light-emitting devices with extended operating lifetimes on plastic substrates, Appl. Phys. Lett. 81 (2002) 2929–2931.
[26] G.L. Graff, R.E. Williford, P.E. Burrows, Mechanisms of vapor permeation through multilayer barrier films: lag time versus equilibrium permeation, J. Appl. Phys. 96 (2004) 1840–1849.
[27] J.-S. Park, H. Chae, H.K. Chung, S.I. Lee, Thin film encapsulation for flexible AM-OLED: a review, Semicond. Sci. Technol. 26 (2011) 34001.
[28] F.M. Elam, S.A. Starostin, A.S. Meshkova, B.C.A.M. van der Velden-Schuermans, J.B. Bouwstra, M.C.M. van de Sanden, H.W. de Vries, Atmospheric pressure roll-to-roll plasma enhanced CVD of high quality silica-like bilayer encapsulation films, Plasma Process. Polym. 14 (2017).
[29] W.A. Pliskin, Comparison of properties of dielectric films deposited by various methods, J. Vac. Sci. Technol. 14 (1977) 1064–1081.
[30] J. Schäfer, R. Foest, A. Quade, A. Ohl, K.-D. Weltmann, Chemical composition of SiO_x films deposited by an atmospheric pressure plasma jet (APPJ), Plasma Process. Polym. 6 (2009) S519–S524.
[31] A. Brunet-Bruneau, J. Rivory, B. Rafin, J.Y. Robic, P. Chaton, Infrared ellipsometry study of evaporated SiO_2 films: matrix densification, porosity, water sorption, J. Appl. Phys. 82 (1997) 1330–1335.
[32] P. Innocenzi, Infrared spectroscopy of sol-gel derived silica-based films: a spectra-microstructure overview, J. Non-Cryst. Solids 316 (2003) 309–319.
[33] J. Schneider, M.I. Akbar, J. Dutroncy, D. Kiesler, M. Leins, A. Schulz, M. Walker, U. Schumacher, U. Stroth, Silicon oxide barrier coatings deposited on polymer materials for applications in food packaging industry, Plasma Process. Polym. 6 (2009) S700–S704.
[34] H.K. Yasuda, Plasma Polymerization, Orlando Academic Press Inc., 1985.
[35] S.A. Starostin, A. Meshkova, F.M. Elam, M.C.M. Van De Sanden, J.B. Bouwstra, H.W. De Vries, Scaling of the atmospheric pressure DBD assisted deposition process for gas diffusion barrier film, 22nd Int. Symp. Plasma Chem., Antwerp, Belgium, 2015.
[36] S.W. Seo, E. Jung, C. Lim, H. Chae, S.M. Cho, Water permeation through organic-inorganic multilayer thin films, Thin Solid Films 520 (2012) 6690–6694.
[37] S. Majee, B. Geffroy, Y. Bonnassieux, J.-E. Bourée, Interface effects on the moisture barrier properties of SiN_x/PMMA/SiN_x hybrid structure, Surf. Coat. Technol. 254 (2014) 429–432.
[38] S. Majee, M.F. Cerqueira, D. Tondelier, B. Geffroy, Y. Bonnassieux, P. Alpuim, J.E. Bourée, Flexible organic-inorganic hybrid layer encapsulation for organic opto-electronic devices, Prog. Org. Coat. 80 (2015) 27–32.
[39] F.M. Elam, S.A. Starostin, A.S. Meshkova, B.C.A.M. van der Velden-Schuermans, M.C.M. van de Sanden, H.W. de Vries, Defect prevention in silica thin films synthesised using AP-PECVD for flexible electronic encapsulation, J. Phys. D. Appl. Phys. 50 (2017).
[40] G. Aresta, P.A. Premkumar, S.A. Starostin, H. De Vries, M.C.M. Van De Sanden, M. Creatore, Optical characterization of plasma-deposited SiO_2-like layers on anisotropic polymeric substrates, Plasma Process. Polym. 7 (2010) 766–774.
[41] D. Shamiryan, M.R. Baklanov, K. Maex, Diffusion barrier integrity evaluation by ellipsometric porosimetry, J. Vac. Sci. Technol., B: Microelectron. Nanometer Struct.–Process., Meas., Phenom. 21 (2003) 220–226.
[42] S.C. Deshmukh, E.S. Aydil, Low - temperature plasma enhanced chemical vapor deposition of SiO_2, Appl. Phys. Lett. 65 (1994) 3185–3187.
[43] M. Creatore, J.C. Cigal, G.M.W. Kroesen, M.C.M. Van De Sanden, Optical and chemical characterization of expanding thermal plasma deposited silicon dioxide-like films, Thin Solid Films 484 (2005) 104–112.
[44] M. Creatore, S.M. Rieter, Y. Barrell, M.C.M. van de Sanden, R. Vernhes, L. Martinu, Optical and chemical characterization of expanding thermal plasma-deposited carbon-containing silicon dioxide-like films, Thin Solid Films 516 (2008) 8547–8553.
[45] L.B. Capeletti, I.M. Baibich, I.S. Butler, J.H.Z. Dos Santos, Infrared and Raman spectroscopic characterization of some organic substituted hybrid silicas, Spectrochim. Acta A Mol. Biomol. Spectrosc. 133 (2014) 619–625.
[46] A.P. Roberts, B.M. Henry, A.P. Sutton, C.R.M. Grovenor, G.A.D. Briggs, T. Miyamoto, M. Kano, Y. Tsukahara, M. Yanaka, Gas permeation in silicon-oxide/polymer (SiO_x/PET) barrier films: role of the oxide lattice, nano-defects and macro-defects, J. Membr. Sci. 208 (2002) 75–88.
[47] A.S. da Silva Sobrinho, G. Czeremuszkin, M. Latrèche, M.R. Wertheimer, Defect-permeation correlation for ultrathin transparent barrier coatings on polymers, J. Vac. Sci. Technol. A 18 (2000) 149–157.
[48] M.C.M. Van De Sanden, Views on macroscopic kinetics of plasma polymerization: acrylic acid revisited, Plasma Process. Polym. 7 (2010) 887–888.
[49] A. von Keudell, J. Benedikt, A physicist's perspective on “views on macroscopic kinetics of plasma polymerisation”, Plasma Process. Polym. 7 (2010) 376–379.